Article

Indium Doping in BaSn$_{3-x}$In$_x$ (0 ≤ x ≤ 0.2) with Ni$_3$Sn Structure

Marion C. Schäfer [1], Yuki Yamasaki [1,2], Veronika Fritsch [3] and Svilen Bobev [1,]*

[1] Department of Chemistry and Biochemistry, University of Delaware, Newark, DE 19716, USA
[2] Department of Chemistry, Hosei University, Tokyo 194-0298, Japan
[3] Physikalisches Institut, Karlsruher Institut für Technologie, D-76131 Karlsruhe, Germany

* Author to whom correspondence should be addressed; E-Mail: bobev@udel.edu;
  Tel.: +1-302-831-8720; Fax: +1-302-831-6335.

Abstract: Investigations of the system Ba–In–Sn, with the objective to synthesize Ba$_8$In$_{16}$Sn$_{30}$ clathrate using Sn and In flux reactions, yielded instead the known BaSn$_3$ compound (*P*6$_3$/*mmc*; *a* = 7.228(2) Å, *c* = 5.469(3) Å) from Sn flux and its In-doped variant BaSn$_{2.8}$In$_{0.2(1)}$ (*a* = 7.260(1) Å, *c* = 5.382(2) Å) from In flux. BaSn$_{3-x}$In$_x$ is the first, and up until now, the only ternary phase containing these elements. Its structure is isomorphic with the Ni$_3$Sn type (Pearson symbol *hP*8) and is apparently capable of sustaining small variations in the valence electron count by virtue of replacing Sn with the electron poorer In. Electrical resistivity measurements on single-crystals of both undoped and doped phases show different metallic-like behavior, suggesting that neither BaSn$_3$ nor BaSn$_{3-x}$In$_x$ are valence compounds.

Keywords: polar intermetallic phases; stannides; barium; tin; crystal structure

1. Introduction

Due to their potential as thermoelectric materials [1,2], intermetallic clathrates (A$_8$[X,Y]$_{46}$)—aka type-I; A$_{24}$[X,Y]$_{136}$)—aka type-II, where A = alkali or alkaline-earth metal; X and Y = groups 13 and 14 elements) have attracted much attention in recent years. Not long ago, our group had reported on several new Si-based clathartes with type-II structure [3]. We were intrigued by the scarcity of isotypic Ge- and particularly Sn-based compounds, with Ba$_{16}$Ga$_{32}$Sn$_{104}$ [4] being the sole example. Our

attention was also piqued by the fact that the system Ba–Ga–Sn appeared carefully mapped out—for example, the polymorphic $Ba_8Ga_{16}Sn_{30}$ clathrate-I and clathrate-VIII compounds [5-7], as well as some other ternary phases like BaGaSn [8], $Ba_3Ga_{0.491}Sn_{4.509}$ [9], and $BaGa_{3.11}Sn_{0.89}$ [10], have been well characterized—while in the Ba–In–Sn system, no ternary phases have been obtained until now.

Therefore, we embarked on systematic investigations of the system Ba–In–Sn. The initial results from our exploratory work in the Sn-rich part of this ternary phase diagram suggested that the known binary phases $BaSn_3$ [11-13] and $BaSn_5$ [11,14] are the most common products of such reactions. Being at the border of the typical intermetallic and Zintl phases, both compounds are reported as superconductors below 2.4 K ($BaSn_3$) and 4.4 K ($BaSn_5$), respectively. The first and only (so far) ternary phase, the solid-solution $BaSn_{3-x}In_x$ was identified from a reaction of the elements using excess In as a metal flux. Its structure is the main subject of this article and was refined from single-crystal X-ray diffraction data; the composition was independently obtained via elemental micro-probe analysis by means of energy-dispersive X-ray spectroscopy (EDX). Electrical resistivity and heat-capacity measurements on single crystals of both phases are also reported.

2. Results and Discussion

During the investigations of the Ba–In–Sn system, single crystals of the known barium tristannide $BaSn_3$ [11-13] and the In-doped barium tristannide $BaSn_{3-x}In_x$ ($x \approx 0.2$) were obtained, instead of the desired, still unknown, clathrates $Ba_8In_{16}Sn_{30}$ or $Ba_{16}In_{32}Sn_{104}$. While $BaSn_3$ can be readily synthesized from elemental mixtures [11-13] or by using Sn flux (this work), $BaSn_{3-x}In_x$ with a small (less than *ca.* 10% at.) substitution of Sn by In was only observed when using large amounts of In as a metal flux. $BaSn_3$ and $BaSn_{3-x}In_x$ both crystallize with the hexagonal space group $P6_3/mmc$ (No. 194) (Pearson symbol $hP8$; Ni_3Sn type structure [15]), the hexagonal variant of the Cu_3Au structure [16]. The structure can be viewed as alternating layers of Ba^{2+} cations (*Wyckoff* site 2*c*: $^1/_3$ $^2/_3$ $^1/_4$) and $[Sn_3]^{2-}$ triangles (*Wyckoff* site 6*h*: 2*x*, *x*, $^3/_4$), as shown in Figure 1. These slabs are arranged in an ABAB sequence along the crystallographic *c*-axis. Since the triangular Sn_3 fragments can also be considered as parts of Sn_6 octahedra that are linked via face-sharing, one can also rationalize the structure as polyanionic 1D-chains along the *c*-axis and Ba^{2+} cations [13]. Full description of the crystal and electronic structure can be found elsewhere [12,13].

The lattice parameters we report for Sn flux-grown $BaSn_3$ are *a* = 7.228(2) Å, *c* = 5.469(3) Å; the literature values for $BaSn_3$ [12,13] are *a* = 7.254(4) and *c* = 5.500(3) Å. These periodicity constants appear to be slightly longer, however, this elongation is not due to any phase width, but to a thermal expansion—our data were obtained at 120(2) K (Table 1), while the previously reported structure was done at room temperature [12,13]. The virtually identical *c*/*a* ratios (0.757 *vs* 0.758) confirm that $BaSn_3$ is a line compound with a robust structure, which is invariant of the method of preparation (stoichiometric reactions vs Sn flux).

However, upon comparison of the above values with the refined unit cell parameters for the "same" compound, grown from In flux, one immediately notices that the structure expands slightly in the *ab*-plane (*a* = 7.260(1) Å) and contracts along the *c* axis (*c* = 5.382(2) Å), which results in significantly smaller *c*/*a* ratio of 0.741, *i.e.*, solid solution $BaSn_{3-x}In_x$ forms. Given the large excess of In employed in the synthesis, we can speculate that the homogeneity range of this phase is rather small,

and that the discussed composition represents the maximum solubility range under these conditions, *i.e.*, $BaSn_{3-x}In_x$ ($0 \leq x \leq 0.2$).

> **Figure 1.** Views of the crystal structure of $BaSn_3$ and $BaSn_{3-x}In_x$, projected along [001] (**a**) and slightly off [110] (**b**). The linkage of the Sn_6 octahedra (and $(Sn,In)_6$, respectively) via face-sharing into infinite chains is emphasized. Ba atoms are drawn as red spheres, and the Sn (or disordered Sn/In) atoms as blue spheres. The thick cylinders between the Sn atoms signify the $[Sn_3]^{2-}$ triangles in the *ab*-planes ($d \approx 3.05$–3.07 Å) and the thin lines represent the longer interlayer bond ($d \approx 3.22$–3.25 Å).
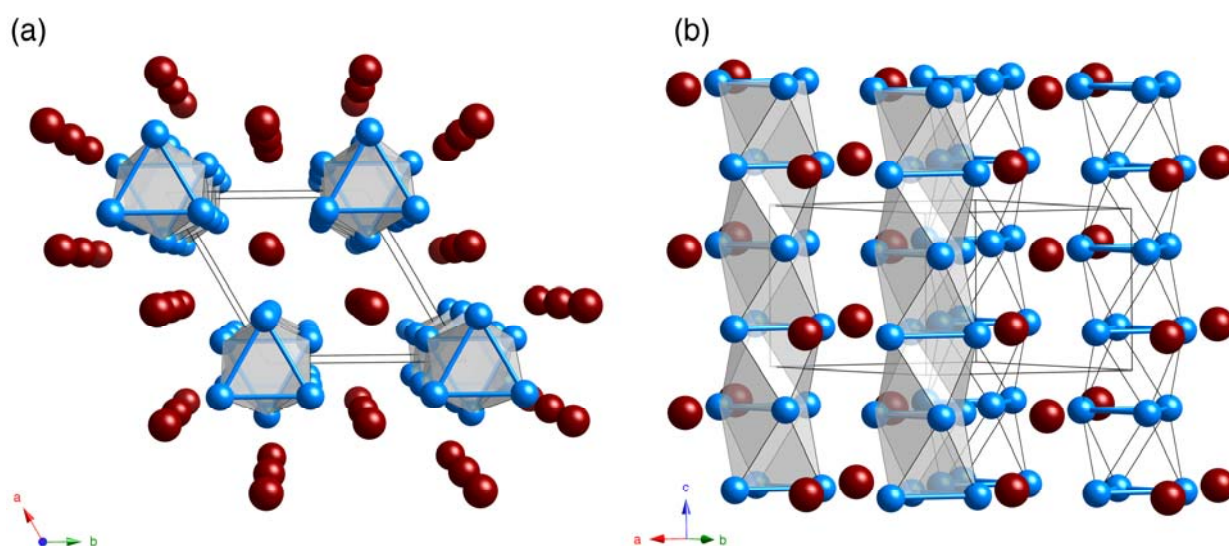
In $BaSn_3$, the Sn–Sn distances within the Sn_3 triangles are 3.051(1) Å, slightly shorter than the corresponding distances in $BaSn_{3-x}In_x$ ($d_{Sn/In-Sn/In} = 3.075(1)$ Å). The opposite trend is observed for the interlayer Sn–Sn distances—they are slightly longer in the pure binary compound ($d_{Sn-Sn} = 3.253$ Å) compared to the In-doped variant ($d_{Sn/In-Sn/In} = 3.224(1)$ Å). The substitution of Sn with In has a very minor effect (or almost no-effect) on the Ba–Sn and Ba–Sn/In distances—$d_{Ba-Sn} = 3.629(1)/3.646(1)$ Å *vs* $d_{Ba-Sn/In} = 3.617(1)/3.644(1)$ Å, respectively. The discussed bond lengths are in good agreement with those reported for other binary compounds like BaSn ($d_{Sn-Sn} = 2.985$ Å; $d_{Ba-Sn} = 3.600$–3.705 Å) [17]; $BaSn_2$ ($d_{Sn-Sn} = 2.919$ Å; $d_{Ba-Sn} = 3.473$ Å) [18], $BaSn_5$ ($d_{Sn-Sn} = 2.959$–3.437 Å; $d_{Ba-Sn} = 3.549$–3.729 Å) [14], and Ba_3Sn_5 ($d_{Sn-Sn} = 2.992$–3.695 Å; $d_{Ba-Sn} = 3.488$–3.731 Å) [19].

Electrical resistivity measurements (Figure 2) for single-crystals of $BaSn_3$ show metallic behavior with ρ_{300K} on the order of 200 μΩ·cm. At temperature below *ca.* 4.5 K, the material undergoes a phase change, following which it becomes superconducting, as evidenced from the abrupt jump in the $\rho(T)$ curve from nearly 12 μΩ·cm to zero resistivity at 3.7 K. This behavior is somewhat puzzling, since superconductivity was reported originally below 2.4 K by *Fässler et al.* [12,13]. Perhaps even more puzzling is the fact that the $\rho(T)$ results are reproducible between crystals from different batches, while heat capacity measurements on the same crystals (supporting information) show no anomalies at this temperature regime. A reasonable interpretation of the data can be accomplished if one recognizes that T_C is very close to the critical temperature of elemental Sn (3.7 K [20]), and since we cannot rule out

the presence of small amounts of free Sn in the $BaSn_3$ specimens grown from Sn flux, most likely this material is not a superconductor.

Figure 2. Temperature dependent electrical resistivity measurements for single-crystals of $BaSn_3$ and $BaSn_{2.8}In_{0.2}$ (Inset: Magnified view of the low temperature region of the resistivity).
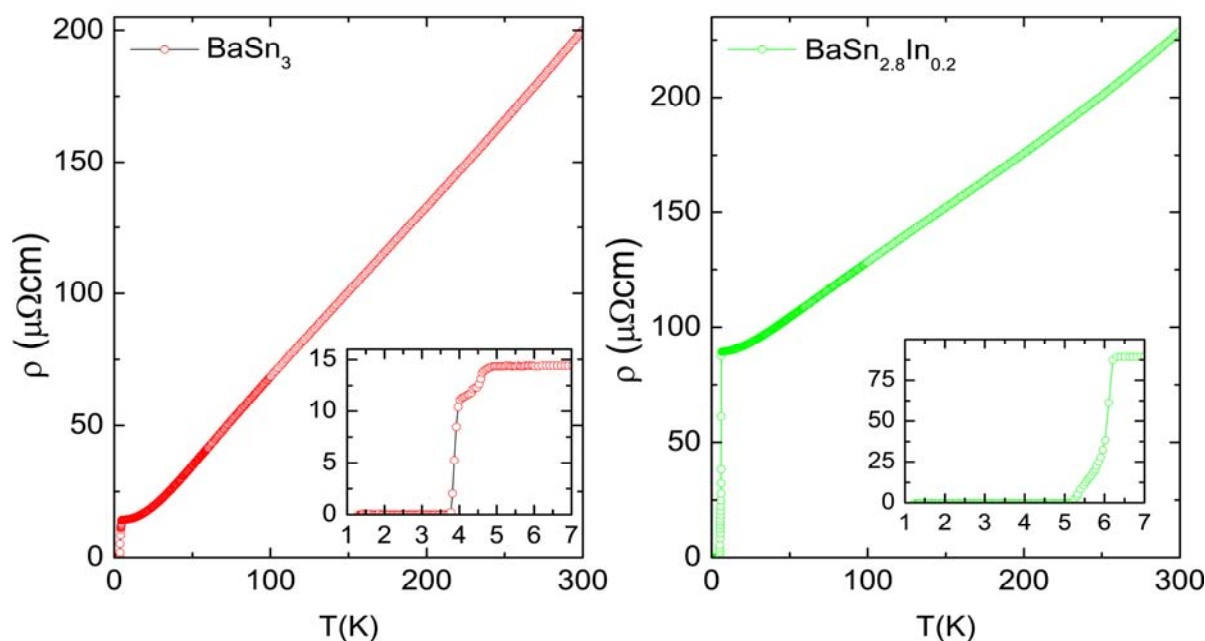
The resistivity of single-crystals of the In-doped $BaSn_{2.8}In_{0.2}$ confirms similar metallic behavior with ρ_{300K} on the order of 230 $\mu\Omega\cdot$cm). This material also becomes a superconductor, but at a higher temperature (*ca.* 6 K). This T_C is 2–3 degrees higher than the critical temperature of elemental Sn (3.7 K [20]) and In (3.4 K [20]), however the heat capacity measurements mirror the behavior observed for $BaSn_3$ and show no anomalies at this temperature regime. Although the $\rho(T)$ behavior of another $BaSn_{3-x}In_x$ sample is similar (T_C is slightly different but the sample might inadvertently has slightly different doping level), the susceptibility data indicate only a small volume fraction. Therefore, we argue that bulk superconductivity is not an intrinsic property of these materials.

3. Experimental Section

Both $BaSn_3$ and $BaSn_{2.8}In_{0.2}$ were obtained using excess of Sn and In as metal fluxes, respectively. In all cases, the corresponding elements (Alfa or Aldrich, purity greater than 99.9%) were loaded in alumina crucibles (2 cm^3) inside an argon-filled glove box. After enclosing the crucibles in evacuated fused silica tubes, they were heated in programmable muffle furnaces to 1000 °C (rate 10 °C/h), equilibrated for 5 h, cooled to 450 °C (rate –300 °C/h) and annealed at 450 °C for 12 h. The flux was removed (by decanting it) subsequent to another cooling step to 400 °C (rate –10 °C/h). The silica tubes were crack-opened in the glove box and the crystals were isolated.

$BaSn_3$ crystals grow very big (up to 7–8 mm long) from Sn flux reactions (loaded in the molar ratio Ba:Sn = 2:15), whereas similar in size crystals of $BaSn_{3-x}In_x$ emerge only from In flux reactions (loaded in the molar ratio Ba:In:Sn = 2:15:7.5). In both cases, the crystals' appear as silver rods.

Extensive efforts to synthesize the desired clathrate $Ba_8In_{16}Sn_{30}$ (or any other ternary phase in this system) have been unsuccessful so far.

X-ray powder diffraction patterns were taken at room temperature on a Rigaku MiniFlex powder diffractometer using Cu Kα radiation. Typical runs included θ–θ scans ($2\theta_{max}$ = 80°) with scan steps of 0.05° and 5 sec/step counting time. The *JADE* 6.5 software package [21] was used for data analysis. The intensities and the positions of the experimentally observed peaks and those calculated from the crystal structures matched very well. Since the diffractometer was enclosed in a nitrogen-filled glove box, we were able to test the air-sensitivity of the title compounds by comparing the diffraction patterns of the freshly prepared samples with those that had been exposed to air. Based on the test results, all of the title compounds are moderately unstable and decompose/hydrolyze after an overnight exposure to air.

Intensity data collections were carried out on a Bruker SMART CCD diffractometer at 120 K using graphite-monochromated Mo-Kα radiation. Suitable single-crystals of $BaSn_3$ and $BaSn_{3-x}In_x$ were selected in a glove box and cut to smaller dimensions (less than 0.1 mm) under mineral oil. The *SMART* [22] and *SAINTplus* [23] programs were used for the data collection, integration and the global unit cell refinement from all data. Semi-empirical absorption correction was applied with *SADABS* [24]. The structures were refined to convergence by full matrix least-square methods on F^2, as implemented in *SHELXTL* [25]. All atoms were refined with anisotropic displacement parameters.

In the refinements of $BaSn_{3-x}In_x$, the Sn atoms, located at *Wyckoff* site 6*h*, were determined to be statistically disordered with a small amount of In (*vide supra*). This was done by freeing the occupation parameter of the Sn site, while keeping the Ba-one fixed, which suggested a slight deviation from full occupancy. Because the X-ray scattering factors for In and Sn are very close, reliable refinements of the composition were not possible and the ratio of Sn to In was established from elemental microanalysis (JEOL 7400F electron microscope equipped with an INCA-OXFORD energy-dispersive spectrometer). In agreement with the averaged ratio of Sn:In = 2.8:0.2, the 6*h* site was assigned as 7 atomic % In and the balance Sn (fixed), yielding a formula $BaSn_{2.8}In_{0.2}$. Selected details of the data collections and structure refinement parameters are summarized in Table 1. The refined atomic coordinates and equivalent isotropic displacement parameters are given in Table 2. Additional details of the crystal structure investigations may be obtained from Fachinformationszentrum Karlsruhe, D-76344 Eggenstein-Leopoldshafen, Germany (Fax: +49-7247-808-666, E-Mail: crysdata@fiz-karlsruhe.de) on quoting the depository numbers CSD-423108 for $BaSn_3$ and CSD-423109 for $BaSn_{2.8}In_{0.2}$, respectively.

Four-probe measurements of the electrical resistivity and heat capacity measurements (thermal relaxation method) as a function of the temperature were carried out on a Quantum Design PPMS system in the interval 2 to 300 K with excitation current of 1 mA. The electrical resistivity was measured on at least two crystals from each batch to assure reproducibility. Polished single crystals were used to minimize geometric errors.

Table 1. Selected crystal data and structure refinement parameters for $BaSn_3$ and $BaSn_{3-x}In_x$.

empirical formula	$BaSn_3$	$BaSn_{2.8}In_{0.2}$
Fw, g/mol	493.41	492.64
Crystal system	Hexagonal	Hexagonal
Space group	$P6_3/mmc$ (No. 194)	$P6_3/mmc$ (No. 194)
a (Å)	7.2279(17)	7.2604(13)
c (Å)	5.4689(26)	5.3817(20)
V (Å^3)	247.43	245.68
Z	2	2
T (K)	120(2)	120(2)
Radiation, λ (Å)	Mo Kα, 0.71073	Mo Kα, 0.71073
ρ (g·cm^{-3})	6.623	6.659
μ (cm^{-1})	226.2	227.0
R_1 [$I > 2\sigma(I)$]^a	0.014	0.021
wR_2 [$I > 2\sigma(I)$]^a	0.030	0.041
largest peak/hole (e$^-$·Å^{-3})	0.45/ −0.84	0.68/ −1.67

^{a} $R_1 = \sum ||F_o| - |F_c||/\sum |F_o|$; $wR_2 = [\sum[w(|F_o^2 - F_c^2|)^2]/\sum[w(F_o^2)^2]]^{1/2}$, where $w = 1/[\sigma^2 F_o^2 + (AP)^2 + BP]$, $P = [F_o^2 + 2F_c^2]/3$; A and B: weight coefficients.

Table 2. Atomic coordinates and equivalent isotropic displacement parameters $(U_{eq})^a$.

Atom	Site^b	x	y	z	U_{eq} (Å^2)
$BaSn_3$					
Ba	$2c$	$^1/_3$	$^2/_3$	$^1/_4$	0.0100(2)
Sn	$6h$	0.7186(1)	0.8593(1)	$^3/_4$	0.0094(2)
$BaSn_{2.8}In_{0.2}$					
Ba	$2c$	$^1/_3$	$^2/_3$	$^1/_4$	0.0085(4)
Sn/In	$6h$	0.7176(1)	0.8588(1)	$^3/_4$	0.0095(3)

^{a} U_{eq} is defined as one third of the trace of the orthogonalized U_{ij} tensor; ^{b} Standardization of the coordinates moves the origin by 0 0 ½ and changes the Wyckoff letter for Ba from $2c$ ($^1/_3$ $^2/_3$ $^1/_4$) to $2d$ ($^1/_3$ $^2/_3$ $^3/_4$). The Wyckoff letter for the Sn (Sn/In) site does not change, but the coordinates become $x = 0.1407(1)$; $y = 0.2814(1)$; $z = ^1/_4$ and $x = 0.1412(1)$; $y = 0.2824(1)$; $z = ^1/_4$, for $BaSn_3$ and $BaSn_{2.8}In_{0.2}$, respectively.

4. Conclusions

Large single-crystals of $BaSn_3$ and $BaSn_{2.8}In_{0.2}$ were obtained using the flux method, following systematic investigations of the Ba–In–Sn ternary diagram. The first and only (so far) ternary phase, the solid-solution $BaSn_{3-x}In_x$ was identified from a reaction of the elements using excess in as a metal flux, while $BaSn_3$ crystals can be readily grown from Sn flux. Both structures were refined from single-crystal X-ray diffraction data and the composition of $BaSn_{2.8}In_{0.2}$ was independently confirmed via energy-dispersive X-ray spectroscopy (EDX). Electrical resistivity measurements on single crystals of both phases indicate metallic behavior in the temperature interval 6–300 K and superconducting behavior below 4–6 K. However, the susceptibility data indicate only a small volume fraction of a superconducting phase in the samples. Based on this, and the fact that the heat capacity measurements

show no anomalies around 2–10 K, we argue that bulk superconductivity is not an intrinsic property of these materials.

Acknowledgments

Supplementary Material

Supplementary data associated with this article can be found in the online version at doi: 10.3390/cryst1030104.

References and Notes

1. Nolas, G.S.; Cohn, J.L.; Slack, G.A.; Schjuman, S.B. Semiconducting Ge clathrates: Promising candidates for thermoelectric applications. *Appl. Phys. Lett.* **1998**, *73*, 178-180.
2. Christensen, M.; Johnson, S.; Iversen, B.B. Thermoelectric clathrates of type I. *Dalton Trans.* **2010**, *39*, 978-992.
3. Bobev, S.; Meyers, J., Jr.; Fritsch, V.; Yamasaki, Y. Synthesis and structural characterization of novel clathrate-II compounds of silicon. *Proc. Int. Conf. Thermoelectr.* **2006**, *25*, 48-52.
4. Kroner, R.; Peters, K.; von Schnering, H.G.; Nespers, R. Crystal structure of the clathrate-II, $Ba_{16}Ga_{32}Sn_{104}$. *Z. Kristallogr. NCS* **1998**, *644*, 664-664.
5. Eisenmann, B.; Schäfer, H.; Zagler, R. Die Verbindungen $A_8B_{16}C_{30}$ (A = Sr, Ba; B = Al, Ga; C = Si, Ge, Sn) und ihre Käfigstrukturen. *J. Less-Common Met.* **1986**, *118*, 43-55.
6. Suekuni, K.; Avila, M.A.; Umeo, K.; Fukuoka, H.; Yamanaka, S.; Nakagawa, T.; Takabatake, T. Simultaneous structure and carrier tuning of dimorphic clathrate $Ba_8Ga_{16}Sn_{30}$. *Phys. Rev.* **2008**, *B77*, 235119.
7. Carrillo-Cabrera, W.; Cardoso Gil, R.H.; Tran, V.H.; Grin, Yu. Refinement of the crystal structure of $Ba_8Ga_{17.2}Sn_{28.8}$. *Z. Kristallogr. NCS* **2002**, *217*, 181-182.
8. Evans, J.E.; Wu, Y.; Kranak, V.F.; Newman, N.; Reller, A.; Garcia-Garcia, F.J.; Häussermann, U. Structural properties and superconductivity in the ternary intermetallic compounds MAB (M = Ca, Sr, Ba; A = Al, Ga, In; B = Si, Ge, Sn). *Phys. Rev.* **2009**, *B80*, 064514.
9. Dürr, I.; Schwarz, M.; Wendorff, M.; Röhr, C. Novel barium triel/tetrelides with the Pu_3Pd_5 structure type. *J. Alloys Compounds* **2010**, *494*, 62-71.
10. Tobash, P.H.; Yamasaki, Y.; Bobev, S. Gallium-tin mixing in $BaGa_{(4-x)}Sn_x$ [$x = 0.89(2)$] with the $BaAl_4$ structure type. *Acta Crystallogr.* **2007**, *E63*, i35-i37.
11. Ray, K.W.; Thompson, R.G. A Study of Barium-Tin Alloys. *Metals Alloys* **1930**, *1*, 314-316.
12. Fässler, T.F.; Kronseder, C. $BaSn_3$: Superconductor at the border of Zintl phases and intermetallic compounds. Real-space analysis of band structures. *Angew. Chem. Int. Ed. Engl.* **1997**, *36*, 2683-2686.

13. Ponou, S.; Fässler, T.F.; Kienle, L. Structural complexity in intermetallic alloys: long-range order beyond 100 nm in the system of BaSn$_3$/BaBi$_3$. *Angew. Chem. Int. Ed. Engl.* **2008**, *47*, 3999-4004.

14. Fässler, T.F.; Hoffmann, S.; Kronseder, C. Novel tin structure motives in superconducting BaSn$_5$- The role of lone pairs in intermetallic compounds (1). *Z. Anorg. Allg. Chem.* **2001**, *627*, 2486-2492.

15. Rahlfs, P. Die Kristallstruktur des Ni$_3$Sn (Mg$_3$Cd-Typ = Überstruktur der hexagonal dichtesten Kugelpackung). *Metallwirtschaft, Metallwissenschaft, Metalltechnik* **1937**, *16*, 343-345.

16. Betteridge, W. Relation between the degree of order and the lattice parameters of Cu$_3$Au. *J. Inst. Met.* **1949**, *75*, 559-570.

17. Rieger, W.; Parthé, E. Alkaline earth silicides, germanides and stannides with CrB structure type. *Acta Crystallogr.* **1967**, *22*, 919-922.

18. Kim S.-J.; Fässler, T.F. Crystal structure of barium distannide, BaSn$_2$. *Z. Kristallogr. NCS* **2008**, *223*, 325-326.

19. Zürcher, F.; Nesper, R.; Hoffmann, S.; Fässler, T. Novel Arachno-type (X$_5$)$^{6-}$ Zintl anions in Sr$_3$Sn$_5$, Ba$_3$Sn$_5$, and Ba$_3$Pb$_5$ and charge influence on Zintl clusters. *Z. Anorg. Allg. Chem.* **2001**, *627*, 2211-2219.

20. Wernick, J.H.; Matthias, B.T. Superconductivity in the In-Sn System. *Chem. Phys.* **1961**, *34*, 2194-2195.

21. *JADE*, Version 6.5; Materials Data, Inc.: Livermore, CA, USA, 2003.

22. *SMART NT*, Version 5.63; Bruker Analytical X-ray Systems Inc.: Madison, WI, USA, 2003.

23. *SAINT NT*, Version 6.45; Bruker Analytical X-ray Systems Inc.: Madison, WI, USA, 2003.

24. *SADABS NT*, Version 2.10; Bruker Analytical X-ray Systems Inc.: Madison, WI, USA, 2001.

25. *SHELXTL*, Version 6.12; Bruker Analytical X-ray Systems Inc.: Madison, WI, USA, 2001.